Finite-temperature dynamics of shock waves in an ultracold Fermi gas

Ria Rushin Joseph,[1] Laura E. C. Rosales-Zárate,[2] and Peter D. Drummond[1]
[1]*Centre for Quantum and Optical Science, Swinburne University of Technology, Melbourne 3122, Australia*
[2]*Centro de Investigaciones en Óptica A.C., León, Guanajuato 37150, México*

(Received 2 June 2018; published 31 July 2018)

The study of finite-temperature dynamics of one-dimensional Fermi gases is a challenging problem. These systems can present different phenomena, including the formation and propagation of shock waves and collective oscillations. Here we calculate the dynamics of collective oscillations and shock waves in a noninteracting one-dimensional ultracold Fermi gas, at both zero and finite temperature. These results are obtained using the Majorana P-function method, which is a positive phase-space representation on a space of antisymmetric matrices. At zero temperature, the results are in agreement with previous results, where the shock wave is observed as a discontinuity of the density of atoms. At finite temperature, the formation of shock waves is observed but with the shock fronts smoothed out. This places constraints on the experimental observation of shock-wave propagation in a noninteracting Fermi gas or strongly interacting Bose gas.

DOI: 10.1103/PhysRevA.98.013638

I. INTRODUCTION

The experimental achievement of Bose-Einstein condensation (BEC) [1–3] and degenerate atomic Fermi gases [4] has opened new areas of research. The study of hydrodynamic properties and nonlinear phenomena in ultracold gases [5,6] has generated considerable recent research interest. Examples of these are the formation of vortices [7–9], solitons [10,11], and shock waves [12–16]. The high controllability achieved in these systems allows one to reduce their dimensionality. In one-dimensional systems, it is possible to observe a Tonks-Girardeau gas [17–20], which is a gas of impenetrable bosons. Due to the Fermi-Bose mapping, this is equivalent to a free Fermi gas [17,21,22].

Shock waves are usually studied in hydrodynamics as a discontinuity of a property of the system. In the case of ultracold atoms shock waves can occur either in a Bose-Einstein condensate [12–15] or in a strongly interacting Fermi gas [16]. For BECs, the dynamics of shock waves have been theoretically studied for one-dimensional gases using a hydrodynamic approach [23,24]. There is also a proposal to generate them in one and two dimensions [25]. For Fermi gases, theoretical work on shock waves have been performed using a hydrodynamic formalism [26,27], a time-dependent superfluid local density approximation [28], an extended density functional approach [29], a generalized nonlinear Schrodinger equation [30], a time-dependent density matrix renormalization group [31], and a time-dependent order parameter equation [32].

Phase-space approaches [33,34] are an alternative method for quantum dynamical simulations of many-body systems. Fermionic phase-space representations have already been used to study the Hubbard model [35–38] and molecular dissociation [39,40]. The advantage of using phase-space techniques is that the underlying space dimension grows quadratically, not exponentially, with the number of modes. A feature of this approach is that since it includes information about the entire many-body density matrix, one can obtain information about higher-order correlation functions as well. This is extremely useful in quantum information applications [41,42]. While other methods are possible for the results obtained in this paper, it is an important proof of principle to apply this technique to problems where it can be compared with existing methods.

Here we study the dynamics of collective oscillations and shock waves in a noninteracting one-dimensional (1D) Fermi gas, both at zero and finite temperature. This is equivalent to a strongly interacting Bose gas in the Tonks-Girardeau limit. We use the Majorana P-function as it can treat any density matrix, is real and positive, and has no sign problem in the cases treated here [36,43,44]. To verify our results, we compare the zero-temperature results with those obtained by Damski [26]. These calculations are then extended to more realistic higher temperatures. We also carry out a quench simulation, giving us the dynamics of collective oscillations for a noninteracting one-dimensional Fermi gas confined in a harmonic trap. At low temperatures, this is also in excellent quantitative agreement with earlier results using a different technique [45].

Both types of dynamical quantum evolution problems treated here are accessible in experiments on ultracold one-dimensional Fermi or Bose gases. In particular, it is important to understand the effects of finite temperatures in these experiments, as true zero-temperature dynamics is not practically accessible. For the shock-wave simulations, we verify earlier predictions of Damski [26] that shock-wave formation occurs in a noninteracting Fermi gas at zero temperature. This is caused by the strong effects of the Pauli exclusion principle, and can be accurately simulated with the P-function techniques described here. It is interesting to observe that these effects, normally regarded as essentially nonlinear in origin, emerge from completely linear phase-space equations. However, we show that an initial finite temperature smooths out the shock-wave fronts, requiring temperatures well below the Fermi temperature where a degenerate Fermi gas is formed, in order to observe them.

This paper is organized as follows: Sec. II describes the Majorana phase-space representations and its time-evolution equation. In Sec. III, we introduce the formalism with a general Hamiltonian as well as particular examples for a given external potential. We use this formalism to describe both the quench dynamics in a 1D harmonic trap and the formation of fermionic shock waves at finite temperature. Section IV gives the simulations of the quench dynamics, which is used to test the method at finite temperatures. Both zero-temperature and finite-temperature shock-wave dynamics are discussed in Sec. V. Section VI gives a summary of our results.

II. MAJORANA QUASIPROBABILITIES

Just as with bosonic quantum fields, fermionic quantum density matrices have more than one quasiprobability distribution in phase space. The Q function is a positive probability distribution that can represent any fermionic quantum density matrix [46]. It is defined as the trace of the product of the density matrix $\hat{\rho}$ and a Gaussian basis. The P function can also represent any fermionic quantum density matrix, but is the complement of the Q function, as it expands the density matrix in terms of the Gaussian basis.

Here we summarize the representation in the case of the Majorana P function [43], which uses a $2M \times 2M$ real antisymmetric matrix $\underline{\underline{x}}$ as the phase-space variable, where M is the number of modes.

A. Definitions

In this section we summarize the formalism of Majorana phase space methods [43] and derive the identities needed for dynamical calculations. We use a diagonal form of the Majorana P function that is defined in a previous work [43], which is an expansion of the density matrix in terms of a basis of Gaussian operators,

$$\hat{\rho} = \int P(\underline{\underline{x}})\hat{\Lambda}(\underline{\underline{x}})d\underline{\underline{x}}. \tag{1}$$

The integration measure is over the antisymmetric matrices satisfying $\underline{\underline{I}} + \underline{\underline{x}}^2 = \underline{\underline{x}}^+\underline{\underline{x}}^- > 0$. This can be extended to complex antisymmetric matrices to give a generalized P function [36,37,47], but this extension is not required here. The unit-trace Majorana Gaussian operator is defined as [44]

$$\hat{\Lambda}(\underline{\underline{x}}) = N(\underline{\underline{x}}) : \exp\{-i\hat{\underline{\gamma}}^T\underline{\underline{\mathcal{I}}}[\underline{\underline{I}} - (\underline{\underline{\mathcal{I}}}\underline{\underline{x}} + \underline{\underline{I}})^{-1}]\hat{\underline{\gamma}}/2\}:. \tag{2}$$

Here, $N(\underline{\underline{x}}) = \frac{1}{2^M}\sqrt{\det[\underline{\underline{\mathcal{I}}} - \underline{\underline{x}}]}$, $\underline{\underline{\mathcal{I}}} = \left[\begin{smallmatrix}\mathbf{0} & \mathbf{I}\\ -\mathbf{I} & \mathbf{0}\end{smallmatrix}\right]$, and $\underline{\underline{I}}$ is the $2M \times 2M$ identity matrix. The Majorana operators $\hat{\underline{\gamma}}$ and $\hat{\underline{\gamma}}^T$ are

$$\begin{aligned}\hat{\underline{\gamma}} &= \underline{\underline{U}}\,\hat{\underline{a}},\\ \hat{\underline{\gamma}}^T &= \hat{\underline{a}}^\dagger\underline{\underline{U}}^\dagger,\end{aligned} \tag{3}$$

where $\hat{\underline{a}} = (\hat{\boldsymbol{a}}^T, \hat{\boldsymbol{a}}^\dagger)^T$ and $\hat{\underline{a}}^\dagger = (\hat{\boldsymbol{a}}^\dagger, \hat{\boldsymbol{a}}^T)$ are $2M$ extended vectors of the creation and annihilation operators. The $\underline{\underline{U}}$ matrix that transforms between Majorana and normal fermionic operators is given by [48]

$$\underline{\underline{U}} = \begin{bmatrix}\mathbf{I} & \mathbf{I}\\ -i\mathbf{I} & i\mathbf{I}\end{bmatrix}. \tag{4}$$

B. Observables

Observables can be calculated in terms of the P function since expectation values of observables O are obtained as [43]

$$\langle O\rangle = \int_{\mathcal{D}_C} P(\underline{\underline{x}}, \tau)\mathrm{Tr}[O\hat{\Lambda}(\underline{\underline{x}})]d\underline{\underline{x}} \equiv \langle O(\underline{\underline{x}})\rangle_P. \tag{5}$$

We use the unordered differential identities derived in [43] to obtain the observable function $O(\underline{\underline{x}})$. We consider the correlation function $\hat{X}_{\mu\nu}$ given by

$$\hat{X}_{\mu\nu} \equiv \frac{i}{2}[\gamma_\mu, \gamma_\nu]. \tag{6}$$

The expectation value of $\hat{X}_{\mu\nu}$ can be calculated using Eq. (5) as

$$\langle\hat{X}_{\mu\nu}\rangle = \frac{i}{2}\int \mathrm{Tr}[\gamma_\mu\gamma_\nu\hat{\Lambda}(\underline{\underline{x}}) - \gamma_\nu\gamma_\mu\hat{\Lambda}(\underline{\underline{x}})]P(\underline{\underline{x}})d\underline{\underline{x}}. \tag{7}$$

We use the following identity [43]:

$$\hat{\underline{\gamma}}\,\hat{\underline{\gamma}}^T\hat{\Lambda} = i\left[\underline{\underline{x}}^-\frac{d\hat{\Lambda}}{d\underline{\underline{x}}}\underline{\underline{x}}^+ - \hat{\Lambda}\underline{\underline{x}}^+\right], \tag{8}$$

where $\underline{\underline{x}}^\pm = \underline{\underline{x}} \pm i\,\underline{\underline{I}}$, in order to obtain

$$\begin{aligned}\langle\widehat{X}_{\mu\nu}\rangle = \frac{1}{2}\int P\mathrm{Tr}\left\{\left[-x^-_{\mu\alpha}\frac{d\hat{\Lambda}}{dx_{\beta\alpha}}x^+_{\beta\nu} + \hat{\Lambda}x^+_{\mu\nu}\right]d\underline{\underline{x}}\right\}\\ -\frac{1}{2}\int P\mathrm{Tr}\left\{\left[-x^-_{\nu\alpha}\frac{d\hat{\Lambda}}{dx_{\beta\alpha}}x^+_{\beta\mu} + \hat{\Lambda}x^+_{\nu\mu}\right]d\underline{\underline{x}}\right\}.\end{aligned} \tag{9}$$

As we can take the operator trace inside the differential and since $\mathrm{Tr}(\hat{\Lambda}) = 1$, the derivative terms are all zero. This simplifies the above expression to

$$\langle\widehat{\underline{\underline{X}}}\rangle = \int \underline{\underline{x}}P(\underline{\underline{x}})d\underline{\underline{x}}. \tag{10}$$

Therefore, $\underline{\underline{x}}$ has a physical interpretation, as its mean value is proportional to a quantum correlation function. In the cases treated here, where the density operator is Gaussian, one can relate the $\underline{\underline{x}}$ variable with correlation functions directly since

$$\underline{\underline{x}} = \begin{bmatrix}i(\mathbf{n}^- + \mathbf{m}^-) & \mathbf{n}^+ + \mathbf{m}^+ - \mathbf{I}\\ -\mathbf{n}^+ + \mathbf{m}^+ + \mathbf{I} & i(\mathbf{n}^- - \mathbf{m}^-)\end{bmatrix}, \tag{11}$$

where $\mathbf{n}^\pm = \mathbf{n} \pm \mathbf{n}^T$, $\mathbf{m}^\pm = \mathbf{m} \pm \mathbf{m}^*$, and $n_{ij} = \langle\hat{a}_i^\dagger\hat{a}_j\rangle$, $m_{ij} = \langle\hat{a}_i\hat{a}_j\rangle$. If, in addition, there are no anomalous correlations, so $\mathbf{m} = \mathbf{0}$, the above expression becomes

$$\underline{\underline{x}} = \begin{bmatrix}i\mathbf{n}^- & \mathbf{n}^+ - \mathbf{I}\\ \mathbf{I} - \mathbf{n}^+ & i\mathbf{n}^-\end{bmatrix}. \tag{12}$$

If $\mathbf{n} = \mathbf{n}^T$, it simplifies further to give

$$\underline{\underline{x}} = \begin{bmatrix}\mathbf{0} & 2\mathbf{n} - \boldsymbol{I}\\ \boldsymbol{I} - 2\mathbf{n} & \mathbf{0}\end{bmatrix}. \tag{13}$$

C. Dynamical evolution

Although the methods we use can treat other Hamiltonians, here as an example we consider number-conserving Hamiltonians of the form

$$\widehat{H} = \hbar\omega_{ij}\widehat{a}_i^\dagger\widehat{a}_j, \tag{14}$$

where i, j are summed over the M system modes.

If we define the Majorana commutator as in Eq. (6) and

$$\underline{\underline{\Omega}} = \begin{bmatrix} 0 & \boldsymbol{\omega} \\ -\boldsymbol{\omega} & 0 \end{bmatrix}, \tag{15}$$

we can reexpress the Hamiltonian in terms of Majorana operators as [43]

$$\hat{H} = \frac{\hbar}{2}\Omega_{\mu\nu}\hat{X}_{\mu\nu}. \tag{16}$$

The time evolution of the Majorana Q function is known to be given by [43]

$$\frac{dQ\left(\underline{x}\right)}{dt} = \Omega_{\mu\nu}\left[\frac{d}{dx_{\nu\kappa}}\left(x_{\mu\kappa}Q\right) - \frac{d}{dx_{\kappa\mu}}\left(x_{\kappa\nu}Q\right)\right]. \tag{17}$$

It is also possible to obtain the time-evolution equation of the P function following a similar strategy to the one used for the Q function. In this case, the time-evolution equation of the density operator is given by

$$i\hbar\frac{\partial}{\partial t}\hat{\rho} = [\hat{H}, \hat{\rho}]. \tag{18}$$

Taking the derivative of (1) with respect to the time gives

$$\frac{\partial}{\partial t}\hat{\rho} = \int \frac{dP}{dt}\hat{\Lambda}dx. \tag{19}$$

From Eqs. (18) and (19), together with the definition of the Hamiltonian given in Eq. (16) and the correlation function of Eq. (6), we get the following time-evolution equation for the Majorana P function:

$$\int \frac{dP}{dt}\hat{\Lambda}dx = \frac{1}{4}\Omega_{\mu\nu}\int P[\gamma_\mu\gamma_\nu - \gamma_\nu\gamma_\mu, \widehat{\Lambda}]dx.$$

We now use the following differential identity [43]:

$$[\gamma_\mu\gamma_\nu - \gamma_\nu\gamma_\mu, \widehat{\Lambda}] = 4\left[x_{\kappa\nu}\frac{d\hat{\Lambda}}{dx_{\kappa\mu}} - x_{\mu\kappa}\frac{d\hat{\Lambda}}{dx_{\nu\kappa}}\right]. \tag{20}$$

After performing an integration by parts and assuming that the boundary terms are zero, we get

$$\frac{dP}{dt} = \Omega_{\mu\nu}\left[\frac{d}{dx_{\nu\kappa}}(x_{\mu\kappa}P) - \frac{d}{dx_{\kappa\mu}}(x_{\kappa\nu}P)\right]. \tag{21}$$

The method of characteristics allows one to solve the above equation, which leads to

$$\frac{d\underline{\underline{x}}}{dt} = [\underline{\underline{\Omega}}, \underline{\underline{x}}]. \tag{22}$$

The final result is in the form of a commutation relation and is the same as that obtained for the Majorana Q function [43]. However, since the initial condition for the P function is a delta function in the cases treated here, only one trajectory is needed, which makes the calculations more efficient. In the cases treated in this paper, we solve these matrix differential equations with the widely used Runge-Kutta 4-5 adaptive algorithm, with a relative error tolerance of $\pm 10^{-3}$ and an absolute error tolerance of $\pm 10^{-6}$ [49,50].

III. HAMILTONIAN

For the initial conditions in these calculations, we treat Fermi systems in a grand-canonical ensemble at finite temperature. The unnormalized quantum density matrix is

$$\hat{\rho} = \exp[-\beta(\hat{H} - \mu\hat{N})], \tag{23}$$

where $\hat{H}$ is the Hamiltonian, $\beta = 1/k_BT$ at temperature T, $\hat{N}$ is the number operator, and the chemical potential μ is chosen so that the mean particle number is $N = \langle\hat{N}\rangle$. This implies that we use the Fermi distribution

$$n_{ij} = \langle\hat{a}_i^\dagger\hat{a}_j\rangle = \frac{\delta_{ij}}{1 + \exp[\beta(E_i - \mu)]}, \tag{24}$$

where E_i is the ith-mode energy, with a corresponding phase-space variable given by Eq. (13). Since the density matrix is a Gaussian operator, it corresponds to a delta function in the real phase space of the Majorana P representation.

A. One-dimensional Fermi gas

In more detail, we consider a one-dimensional noninteracting Fermi gas, which is trapped in a box of length $L = 2l$, extending from $-l$ to l. Throughout the paper, we use the following convention for units: $m = \hbar = k_B = 1$. This leaves a single length scale ℓ_0, which can be chosen arbitrarily. We define all distances as dimensionless in terms of this length scale, so that $z = \boldsymbol{r}_3/\ell_o$. One can also regard this as a choice of the unit of time as $t_0 = m\ell_0^2/\hbar$, so we define t in terms of these units.

The model Hamiltonian is

$$\widehat{H} = \hat{H}_0 + \int_{-l}^{l} dz V(z)\psi^\dagger(z)\psi(z), \tag{25}$$

where $V(z)$ is the external potential and $\hat{H}_0$ is the Hamiltonian without perturbation,

$$\hat{H}_0 = \sum_k \omega_k\hat{a}^\dagger(k)\hat{a}(k). \tag{26}$$

The Hamiltonian $\hat{H}$ is in position space. It is useful to convert it into momentum space, where one can define [51]

$$\psi(z) = \frac{1}{\sqrt{L}}\sum_{k'} e^{ik'z}\hat{a}_{k'}. \tag{27}$$

Utilizing this relation, the Hamiltonian in momentum space is

$$\hat{H} = \hat{H}_0 + \hat{H}_e, \tag{28}$$

where

$$\hat{H}_e = \frac{1}{L}\sum_{k,k'}\hat{a}_k^\dagger\hat{a}_{k'}\int dz V(z)e^{i(k'-k)z}. \tag{29}$$

After performing the integration, we can express the Hamiltonian in the following concise form:

$$\hat{H} = \sum_{kk'}\hbar\omega_{kk'}\widehat{a}_k^\dagger\widehat{a}_{k'}. \tag{30}$$

We note that this Hamiltonian has an identical form to that given in Eq. (14), and thus we can use the differential equations obtained for the P function, given in Eq. (22), to simulate the dynamics of a Fermi gas at any temperature. This includes the formation of shock waves or other dynamics. In this case, the elements of the matrix $\underline{\underline{\Omega}}$ are given in Eq. (15).

The momentum correlation function $n_{kk'}$ is then obtained from the phase-space distribution using Eq. (24), which can be used to calculate the density of atoms in position space, $n(z)$:

$$n(z) = \langle \psi^\dagger(z)\psi(z)\rangle. \tag{31}$$

Using the definition of $\psi(z)$ given in Eq. (27), we obtain

$$n(z) = \left\langle \frac{1}{L}\sum_{k,k'} e^{i(k'-k)z}\hat{a}_k^\dagger \hat{a}_{k'} \right\rangle = \frac{1}{L}\sum_{k,k'} e^{i(k'-k)z} n_{kk'}. \tag{32}$$

As an example, we analyze two models whose formalism is similar. The first model has a variable harmonic-oscillator potential, and the second model is a 1D Fermi gas trapped in a box, with an external laser to give an additional localized trap that is used to generate the low-temperature shock waves.

B. Harmonic trap

For investigating the collective oscillation quench, we consider a one-dimensional Fermi gas trapped in a harmonic potential of the form

$$V(z) = \tfrac{1}{2}\omega^2 z^2, \tag{33}$$

where ω is the trapping frequency that is changed in time during the quench.

We use this external potential in order to perform the integral of Eq. (29) from $-l$ to l, with a total length $L = 2l$, obtaining

$$\widehat{H}_e = \frac{\omega^2}{2L}\sum_{kk'} \hat{a}_k^\dagger \hat{a}_{k'} \{A_{kk'}\cos[l(k'-k)] - B_{kk'}\sin[l(k'-k)]\}, \tag{34}$$

where $A_{kk'} = 4l(\frac{1}{k'-k})^2$ and $B_{kk'} = 4(\frac{1}{k'-k})^3 - 2l^2(\frac{1}{k'-k})$. This expression is valid only for $k \neq k'$. In the case that $k = k'$, we get

$$A_{kk} = \frac{2l^3}{3}. \tag{35}$$

Using these expressions, the explicit form of the Hamiltonian in Eq. (30) is

$$\widehat{H} = \sum_k \omega_k \widehat{a}^\dagger(k)\widehat{a}(k) + \frac{\omega^2}{2L}\sum_{kk'} \widehat{a}_k^\dagger \widehat{a}_{k'} \times \{A_{kk'}\cos[l(k'-k)] - B_{kk'}\sin[l(k'-k)]\}. \tag{36}$$

Hence, for this case the frequency matrix $\omega_{kk'}$ is

$$\omega_{kk'} = \begin{cases} \omega_k + \omega^2 l^2/6, & k = k', \\ \{A_{kk'}\cos[l(k'-k)] - B_{kk'}\sin[l(k'-k)]\}\frac{\omega^2}{4l}, & k \neq k', \end{cases} \tag{37}$$

with

$$\omega_k = \frac{k_n^2}{2}, \tag{38}$$

where $k \equiv k_n = (n - n_0)\Delta k$ and k_n is symmetric by choosing

$$n_0 = \frac{M-1}{2}, \quad n = 0, 1, \ldots, M-1.$$

C. Perturbed flat potential

For investigating shock waves, we now consider a flat potential with a time-varying Gaussian perturbation caused by an external dipole coupled laser input,

$$V(z) = u_0\alpha(t)\exp\left[-\frac{\alpha(t)z^2}{2\sigma^2}\right]. \tag{39}$$

Here, $\alpha(t) = t/t_f$, t_f is the final time, and u_0 and σ are the height and width of the potential, respectively. When we perform the integral of Eq. (29) in the limit that $\sigma << L$, using the external potential given in Eq. (39), we get

$$\widehat{H} = \widehat{H}_0 + \frac{u_0\sigma}{L}\sqrt{2\pi\alpha(t)}\sum_{k,k'} \hat{a}_k^\dagger \hat{a}_{k'} \exp\left[-\frac{\sigma^2(k'-k)}{2\alpha(t)}\right]. \tag{40}$$

The frequency matrix $\omega_{kk'}$ in Eq. (30) can then be defined as

$$\omega_{kk'} = \delta_{kk'}\omega_k + \frac{u_0\sigma}{L}\sqrt{2\pi\alpha(t)}\exp\left[-\frac{\sigma^2(k'-k)}{2\alpha(t)}\right]. \tag{41}$$

Here, ω_k is the same free particle energy as in Eq. (38).

IV. QUENCH DYNAMICS

To illustrate the use of Majorana P functions in a finite-temperature dynamical simulation, we first consider the problem of a quantum many-body bounce or collective oscillation in an external harmonic potential, which has been treated previously using different techniques [45]. The quench dynamics is obtained when the trapping frequency ω is changed instantaneously from an initial value of $\omega_0 = 1$ to a final value of $\omega_1 = \omega_0/6$ at time $t = 0$, with a quench strength of $\epsilon = \omega_0^2/\omega_1^2 - 1 = 35$ [45]. In this case, the initial value of the correlation matrix can be calculated as

$$n_{k'k} = \sum_n \sum_m \langle \hat{b}_n^\dagger \hat{b}_m\rangle^{HO} \phi_n^\dagger(k')\phi_m(k), \tag{42}$$

where for a noninteracting Fermi gas at temperature T,

$$\langle \hat{b}_n^\dagger \hat{b}_m\rangle^{HO} = \frac{\delta_{nm}}{1 + \exp[\beta(E_n - \mu)]}. \tag{43}$$

Here, $E_n = (n + \frac{1}{2})\omega_0$ are the eigenvalues of the harmonic oscillator. The corresponding eigenstates in momentum space are given by

$$\phi_n(k) = \frac{(-i)^n}{\sqrt{2^n n!}}\left(\frac{1}{\pi\omega_0}\right)^{\frac{1}{4}} e^{-\frac{k^2}{2\omega_0}} H_n\left(\frac{k}{\sqrt{\omega_0}}\right), \tag{44}$$

where $H_n(k)$ are the Hermite polynomials. The chemical potential μ of a Fermi system in a one-dimensional harmonic trap at finite temperature T is given approximately by $\mu = T\ln(e^{T_F/T} - 1)$, where $T_F = N\omega_0$, and the discrete summations are replaced by an integral [52].

We study the dynamics of the system by solving Eq. (22). The initial value of the $\underline{\underline{x}}$ matrix is given in Eq. (13) and is obtained from the correlation matrix of Eq. (42). The elements

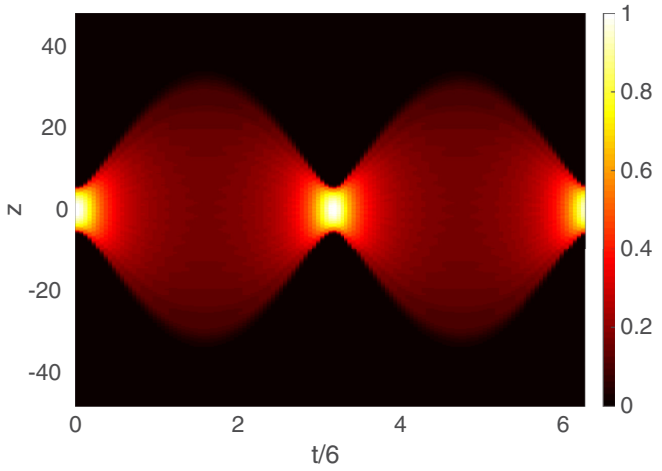

FIG. 1. Normalized density of atoms in position space of a 1D Fermi gas with dimensionless initial temperature of $\theta_0 = 0.01$, $N = 16$, $M = 401$, $\epsilon = 35$.

of the matrix $\underline{\underline{\Omega}}$ are given in Eq. (37). In this form, we obtain the matrix $\underline{\underline{x}}(t)$ as a function of time, which allows us to calculate the correlation matrix at different times. The density of atoms in position space is then evaluated using the expression given in Eq. (32). We use the harmonic-oscillator scale of length, with $\sqrt{1/\omega_0} = 1$, and we also introduce a scaled temperature relative to the Fermi temperature, $\theta_0 = T/T_F$.

Figures 1 and 2 show the normalized density of atoms in position space obtained from the formalism described above for the Majorana P function for two different values of θ_0, a very low temperature of $\theta_0 = 0.01$, and a higher temperature of $\theta_0 = 0.5$, near the Fermi degeneracy temperature. We observe the dynamics of breathing modes. These results are in excellent agreement with those obtained by Atas *et al.* [45] for a Tonks-Girardeau gas, who used a different approach based on the Bose-Fermi mapping and the Fredholm determinant.

We also checked our low-temperature results by comparing them with known analytic zero-temperature results. This

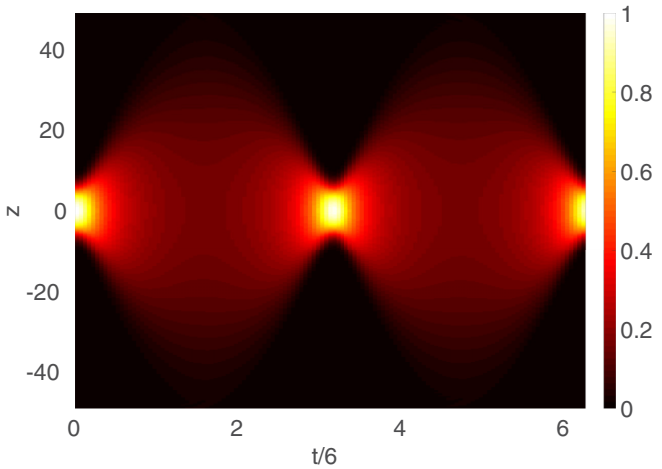

FIG. 2. Normalized density of atoms in position space of a 1D Fermi gas with dimensionless initial temperature of $\theta_0 = 0.5$, $N = 16$, $M = 401$, $\epsilon = 35$.

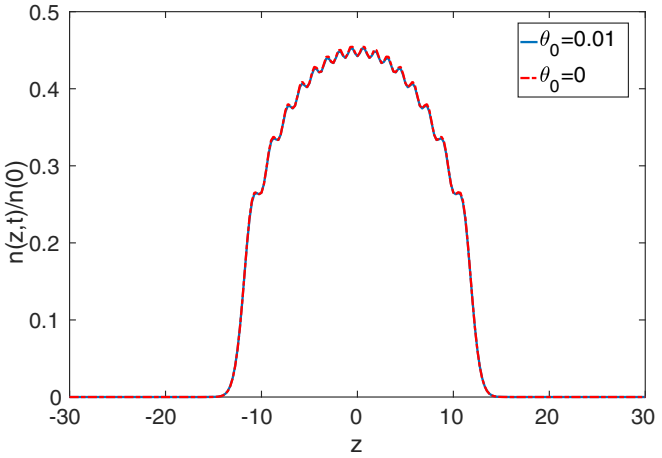

FIG. 3. Normalized density of atoms in position space for a 1D Fermi gas. Here we used $N = 16$, $M = 401$, and $\epsilon = 35$ at time $\omega_1 t = 2.1$.

comparison is valid since we consider a finite temperature of $\theta_0 = 0.01$, which is well below the Fermi temperature. The expression for the density of atoms at zero temperature in a time-dependent harmonic trap when considering a quench is given by [45]

$$n(z,t) = \frac{1}{\lambda} n\left(\frac{z}{\lambda}\right), \tag{45}$$

where

$$n(z) = \frac{e^{-z^2}}{\sqrt{\pi}} \sum_{n=0}^{N-1} \frac{H_n^2(z)}{2^n n!},$$

and the scaling term is $\lambda(t) = [1 + \epsilon \sin^2(\omega_1 t)]^{\frac{1}{2}}$ [45]. In the case where there is no quench, i.e., $\epsilon = 0$, this expression reduces to the standard ground-state density distribution.

Figure 3 shows the normalized density of atoms in position space, given by Eq. (32), at a fixed dimensionless time of $\omega_1 t = 2.1$ and a finite temperature of $\theta_0 = 0.01$ (blue solid line). We also plot the exact density of atoms for zero temperature at the same time (red dashed line) using Eq. (45). In this case, as we expected, we obtain an excellent agreement between these results since the temperature is far below the Fermi temperature. In Fig. 4, we also plot a comparison of the normalized density of atoms in position space for zero temperature (red dashed line) but with a higher temperature of $\theta_0 = 0.5$ (blue solid line). This gives us a temperature $T \sim T_F/2$ and shows that the P function can simulate the finite-temperature dynamics of a Fermi gas in a regime where the two results are expected to strongly differ.

V. SHOCK-WAVE DYNAMICS

The dynamics of shock waves in a 1D Fermi gas trapped in a periodic box can also be described using the fermionic P function. Here we wish to simulate the complete cycle that could be used experimentally for a finite-temperature experiment to observe shock waves, keeping in mind that a zero-temperature noninteracting Fermi gas is difficult to obtain. We assume that the localized, trapped atom system in

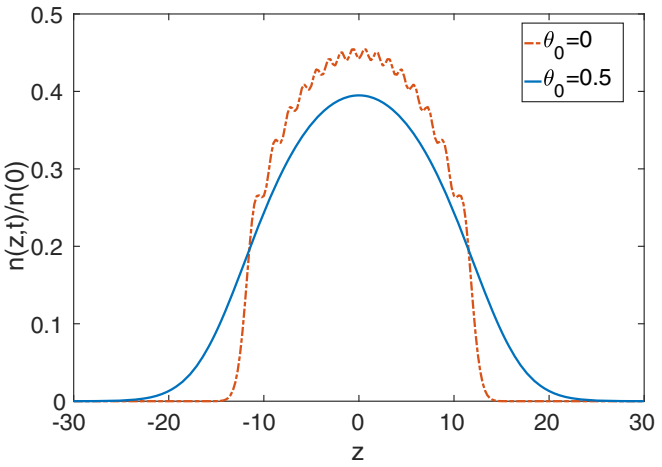

FIG. 4. Normalized density of atoms in position space for a 1D Fermi gas. Parameters are the same as in Fig. 3.

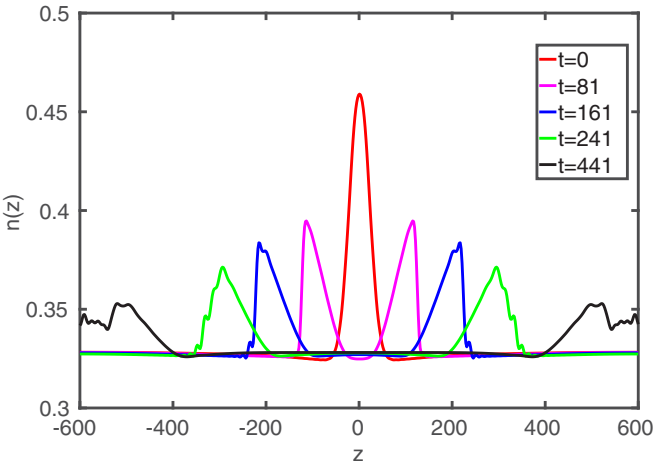

FIG. 5. Zero-temperature dynamics of shock waves: Density of atoms as a function of position at different times. Parameters: $M = 600$, $u_0 \approx -0.53$, $\sigma = 20$, $N = 399$, $l = 600$.

a Gaussian dipole potential—from a focused laser beam—is obtained using an adiabatic passage from a larger, nearly uniform sample of the trapped gas at finite temperature.

In this case, the density of atoms as a function of time and position is obtained by performing the simulation in two stages. First, the trapping laser is turned on adiabatically from a known untrapped thermal state in order to obtain a finite-temperature equilibrium state. Thus, we solve the differential equations of Eq. (22), using the initial condition for the $\underline{x}$ matrix given in Eq. (13) and the correlation matrix of Eq. (24). This corresponds to a quasithermal density matrix, in the sense that the corresponding distribution of thermal states in the laser potential has the same entropy as the initial Fermi-Dirac distribution. We note that faster methods may be available, although these are often limited to special types of external potential, such as the harmonic potentials of the previous section [53].

Next, for the dynamical stage, the solution obtained in the adiabatic stage at the final time is used as the initial condition. We solve the differential equations by switching off the laser potential, obtaining the values of the $\underline{x}$ matrix at different times. Using these values of $\underline{x}$, we can calculate the value of the correlation matrix. Substituting these values in the expression for the density of atoms given in Eq. (32) leads to the dynamics of the system and, in the course of time evolution, we can observe the formation of shock waves.

The numerical results using this phase-space approach are shown below for zero and finite temperature. In order to perform the calculations, we assume that the boundaries of the 1D periodic box are $z = \pm l$ [26]. Here, as previously, ℓ_0 is an arbitrary unit of length used to make the equations dimensionless. For the purpose of comparison, we use the same parameters and units as in [26].

The chemical potential of the original 1D Fermi gas confined in a box at zero temperature is given by $\mu = E_N - E_0 = \omega_N - \omega_0$, and hence

$$\mu = \frac{N^2 \triangle k^2}{8}, \tag{46}$$

where N is the number of Fermi particles. For finite temperatures T, the chemical potential is [54]

$$\mu = \epsilon_F \left[1 + \left(\frac{\pi^2}{12} \right) \left(\frac{T}{T_F} \right)^2 \right]. \tag{47}$$

A. Zero-temperature results

The numerical simulations are performed as described previously. Here we have used an adiabatic stage with a total elapsed time of $t_f = 6001$, while for the dynamical stage we have used $t_f = 1000$. The adiabatic stage uses the Fermi-Dirac distribution as the initial condition. At zero temperature, this is given by

$$n_{ij} = \langle \hat{a}_i^\dagger \hat{a}_j \rangle = \begin{cases} 1 & \text{if } \omega_i < \mu \\ 0 & \text{if } \omega_i > \mu. \end{cases}$$

In Fig. 5, we show the results for the dynamics of shock waves for different times in dimensionless time units. Here we consider the initial time $t = 0$. We show the different density

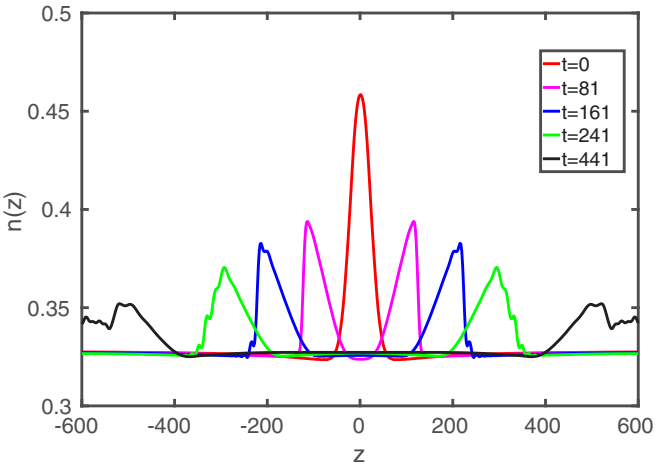

FIG. 6. Dynamics of shock waves at different times for a finite temperature $\theta = 0.005$. Other parameters are the same as in Fig. 5.

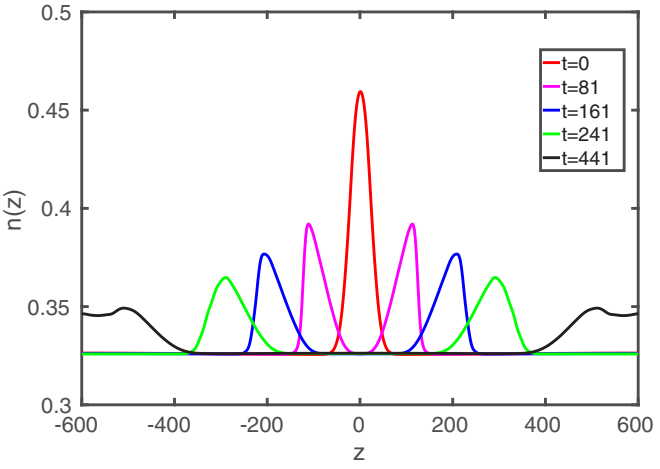

FIG. 7. Dynamics of shock waves at different times for a finite temperature $\theta = 0.07$. Other parameters are the same as in Fig. 5.

profiles for different times up to a final time. The initial density profile has a Gaussian shape as expected. As time progresses, the density of atoms splits into two parts. The upper half of each half wave moves faster than the lower part, which leads to the formation of shock waves.

B. Finite-temperature results

In any realistic Fermi gas experiment, the temperature will not be zero. It is an open question as to what happens in this case. We have performed the shock-wave simulations for different values of the initial temperature. To define a suitable dimensionless scale, we choose a scaled temperature as $\theta = \frac{T}{T_F}$, noting that here both T and T_F refer to the initial thermal equilibrium Fermi gas before adiabatic passage.

In Figs. 6–8, we show the density of atoms as a function of position at different times for different values of temperature, $\theta \in (0.005\text{–}0.2)$. The plots show the shock-wave dynamics of a 1D Fermi gas subject to a perturbed flat potential. For $t = 0$, the initial density profile has a Gaussian pattern. As the time

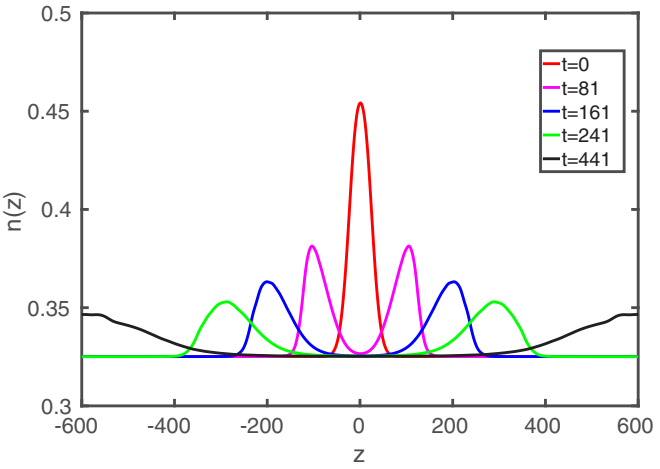

FIG. 8. Dynamics of shock waves at different times for a finite temperature $\theta = 0.2$. Other parameters are the same as in Fig. 5.

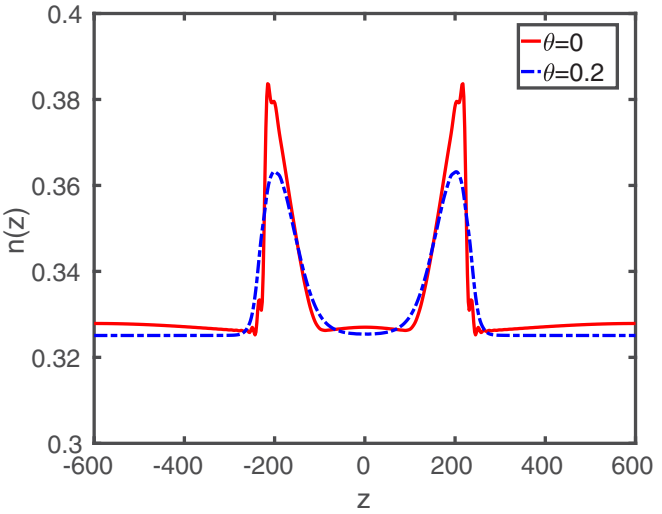

FIG. 9. Effect of temperature on the dynamics of shock waves. Here we have considered both zero temperature and finite temperature, with $\theta = 0.2$, at a time $t = 161$. Other parameters are the same as in Fig. 5.

advances, this Gaussian pattern splits into two parts, which move in two different directions as previously. We notice that as the temperature increases, it is more difficult to observe the shock-wave characteristic behavior of a vertical leading edge. Hence our results show that the effect of the temperature is to smooth out the sharp leading edges, which makes these shock-wave effects harder to observe as the temperature increases.

This effect is observed clearly in Fig. 9, where we plot the density of atoms for zero temperature and a higher temperature of $\theta = 0.2$, at a fixed time of $t = 161$. Since this is only 20% of the original Fermi temperature, we predict that shock-wave observations of this type will require an extremely degenerate initial atomic Fermi gas.

VI. SUMMARY

We have shown that by utilizing the fermionic P-function method, together with Majorana unordered differential identities [43], one can calculate in detail the dynamics of density wave packets in a Fermi gas. This method is relatively simple to implement, and takes advantage of the mappings between the fermionic Hilbert space, and the Lie group of antisymmetric matrices. It has been applied to study the dynamics of a Fermi gas at zero and finite temperature. We have verified our results for the dynamics of the 1D harmonically trapped Fermi gas by comparison with previous results [45]. We expect this approach to have wider applications to the physics and both coherent and decoherent evolution of Majorana excitations in a fermionic condensed-matter system as well.

We have used this method to simulate the dynamics of fermionic shock waves at zero and finite temperatures. This prediction can be tested in one-dimensional Fermi or Bose gas experiments by using Feshbach resonances to tune the interaction strength to either zero or very high values, respectively. Last, we have found that the "quantum" shock-wave front decays smoothly in finite-temperature dynamics, instead

of creating a sharp front in the course of its time evolution. This effect is more pronounced at finite temperature and leads to stringent requirements on temperature for fermionic shock waves.

ACKNOWLEDGMENTS

We thank Y. Atas for useful correspondence. R.R.J. acknowledges financial support from a Victoria India Doctoral scholarship.

[1] C. C. Bradley, C. A. Sackett, J. J. Tollett, and R. G. Hulet, Phys. Rev. Lett. **75**, 1687 (1995).
[2] M. H. Anderson, J. R. Ensher, M. R. Matthews, C. E. Wieman, and E. A. Cornell, Science **269**, 198 (1995).
[3] K. B. Davis, M. O. Mewes, M. R. Andrews, N. J. van Druten, D. S. Durfee, D. M. Kurn, and W. Ketterle, Phys. Rev. Lett. **75**, 3969 (1995).
[4] B. DeMarco and D. S. Jin, Science **285**, 1703 (1999).
[5] I. Bloch, J. Dalibard, and W. Zwerger, Rev. Mod. Phys. **80**, 885 (2008).
[6] S. Giorgini, L. P. Pitaevskii, and S. Stringari, Rev. Mod. Phys. **80**, 1215 (2008).
[7] M. R. Matthews, B. P. Anderson, P. C. Haljan, D. S. Hall, C. E. Wieman, and E. A. Cornell, Phys. Rev. Lett. **83**, 2498 (1999).
[8] K. W. Madison, F. Chevy, W. Wohlleben, and J. Dalibard, Phys. Rev. Lett. **84**, 806 (2000).
[9] M. W. Zwierlein, J. R. Abo-Shaeer, A. Schirotzek, C. H. Schunck, and W. Ketterle, Nature (London) **435**, 1047 (2005).
[10] S. Burger, K. Bongs, S. Dettmer, W. Ertmer, K. Sengstock, A. Sanpera, G. V. Shlyapnikov, and M. Lewenstein, Phys. Rev. Lett. **83**, 5198 (1999).
[11] J. Denschlag *et al.*, Science **287**, 97 (2000).
[12] Z. Dutton, M. Budde, C. Slowe, and L. V. Hau, Science **293**, 663 (2001).
[13] M. A. Hoefer, M. J. Ablowitz, I. Coddington, E. A. Cornell, P. Engels, and V. Schweikhard, Phys. Rev. A **74**, 023623 (2006).
[14] J. J. Chang, P. Engels, and M. A. Hoefer, Phys. Rev. Lett. **101**, 170404 (2008).
[15] R. Meppelink, S. B. Koller, J. M. Vogels, P. van der Straten, E. D. van Ooijen, N. R. Heckenberg, H. Rubinsztein-Dunlop, S. A. Haine, and M. J. Davis, Phys. Rev. A **80**, 043606 (2009).
[16] J. A. Joseph, J. E. Thomas, M. Kulkarni, and A. G. Abanov, Phys. Rev. Lett. **106**, 150401 (2011).
[17] M. Girardeau, J. Math. Phys. **1**, 516 (1960).
[18] B. Paredes, A. Widera, V. Murg, O. Mandel, S. Folling, I. Cirac, G. V. Shlyapnikov, T. W. Hansch, and I. Bloch, Nature (London) **429**, 277 (2004).
[19] T. Kinoshita, T. Wenger, and D. S. Weiss, Science **305**, 1125 (2004).
[20] B. Laburthe Tolra, K. M. O'Hara, J. H. Huckans, W. D. Phillips, S. L. Rolston, and J. V. Porto, Phys. Rev. Lett. **92**, 190401 (2004).
[21] M. Olshanii, Phys. Rev. Lett. **81**, 938 (1998).
[22] E. B. Kolomeisky, T. J. Newman, J. P. Straley, and X. Qi, Phys. Rev. Lett. **85**, 1146 (2000).
[23] B. Damski, Phys. Rev. A **69**, 043610 (2004).
[24] B. Damski, Phys. Rev. A **73**, 043601 (2006).
[25] V. M. Pérez-García, V. V. Konotop, and V. A. Brazhnyi, Phys. Rev. Lett. **92**, 220403 (2004).
[26] B. Damski, J. Phys. B **37**, L85 (2004).
[27] L. Salasnich, Europhys. Lett. **96**, 40007 (2011).
[28] A. Bulgac, Y.-L. Luo, and K. J. Roche, Phys. Rev. Lett. **108**, 150401 (2012).
[29] F. Ancilotto, L. Salasnich, and F. Toigo, Phys. Rev. A **85**, 063612 (2012).
[30] N. K. Lowman and M. A. Hoefer, Phys. Rev. A **88**, 013605 (2013).
[31] S. Peotta and M. Di Ventra, Phys. Rev. A **89**, 013621 (2014).
[32] W. Wen, T. Shui, Y. Shan, and C. Zhu, J. Phys. B **48**, 175301 (2015).
[33] M. Hillery, R. F. O'Connell, M. O. Scully, and E. P. Wigner, Phys. Rep. **106**, 121 (1984).
[34] A. Polkovnikov, Ann. Phys. **325**, 1790 (2010).
[35] J. F. Corney and P. D. Drummond, Phys. Rev. Lett. **93**, 260401 (2004).
[36] J. F. Corney and P. D. Drummond, Phys. Rev. B **73**, 125112 (2006).
[37] T. Aimi and M. Imada, J. Phys. Soc. Jpn. **76**, 084709 (2007).
[38] P. Corboz, M. Ögren, K. Kheruntsyan, and J. F. Corney, in *Quantum Gases: Finite Temperature and Non-Equilibrium Dynamics*, Vol. 1 Cold Atoms Series, edited by N. P. Proukakis, S. A. Gardiner, M. J. Davis, and M. H. Szymanska (Imperial College Press, London, 2013).
[39] M. Ögren, K. Kheruntsyan, and J. F. Corney, Comput. Phys. Commun. **182**, 1999 (2011).
[40] M. Ögren, K. Kheruntsyan, and J. F. Corney, Europhys. Lett. **92**, 36003 (2010).
[41] M. D. Reid, B. Opanchuk, L. Rosales-Zárate, and P. D. Drummond, Phys. Rev. A **90**, 012111 (2014).
[42] L. Rosales-Zárate, B. Opanchuk, P. D. Drummond, and M. D. Reid, Phys. Rev. A **90**, 022109 (2014).
[43] R. R. Joseph, L. E. C. Rosales-Zárate, and P. D. Drummond, J. Phys. A **51**, 245302 (2018).
[44] J. F. Corney and P. D. Drummond, J. Phys. A **39**, 269 (2006).
[45] Y. Y. Atas, D. M. Gangardt, I. Bouchoule, and K. V. Kheruntsyan, Phys. Rev. A **95**, 043622 (2017).
[46] L. E. C. Rosales-Zárate and P. D. Drummond, New J. Phys. **17**, 032002 (2015).
[47] P. D. Drummond and C. W. Gardiner, J. Phys. A **13**, 2353 (1980).
[48] R. Balian and E. Brezin, Il Nuovo Cimento B **64**, 37 (1969).
[49] J. R. Dormand and P. J. Prince, J. Comput. Appl. Math. **6**, 19 (1980).
[50] L. F. Shampine and M. W. Reichelt, SIAM J. Sci. Comput. **18**, 1 (1997).
[51] P. D. Drummond and M. Hillery, *The Quantum Theory of Nonlinear Optics* (Cambridge University Press, Cambridge, 2014) .
[52] C. E. Mungan, Eur. J. Phys. **30**, 1131 (2009).
[53] X. Chen, A. Ruschhaupt, S. Schmidt, A. del Campo, D. Guéry-Odelin, and J. G. Muga, Phys. Rev. Lett. **104**, 063002 (2010).
[54] F. J. Sevilla, J. Thermodynam. **2017**, 3060348 (2017).